Wafer scale-up and emergence of ferromagnetism in superhard Q-carbon coatings by nanosecond pulsed laser irradiation

Siddharth Gupta[1], Ritesh Sachan[2], Jagdish Narayan[1]

[1] Department of Materials Science and Engineering, Centennial Campus

North Carolina State University, Raleigh, NC 27695-7907, USA

[2]Department of Mechanical Engineering, Oklahoma State University

ABSTRACT

Laser irradiation has opened an exciting new dimension in materials physics by the transient melting of materials and subsequent ultrafast quenching. Such quenching can generate very high temperatures, leading to the formation of metastable materials like Q-carbon and diamond. Since this transformation is undercooling dependent, we control the undercooling by changing thermal conductivity and sp^3 content in as-deposited amorphous carbon. This study illustrates wafer-scale growth of diamond-like carbon (DLC) thin films by utilizing the pulsed laser deposition technique. By optimizing plume energetics, uniformity in sp^3 composition (40%) of DLC films was achieved which led to the formation of Q-carbon over a large area. We observe room-temperature ferromagnetism in Q-carbon with 140 Oe coercivity and 20 $emug^{-1}$ saturation magnetization. As Q-carbon is harder than diamond, it makes an excellent reinforcing component inside the softer matrix in a composite. These nanocomposites consist of densely-packed sp^3-rich Q-carbon (82% sp^3), and sp^2-rich α-carbon (40% sp^3) amorphous phases. The Q-carbon nanocomposites exhibit a hardness of 67 GPa (Young's modulus ~840 GPa), in contrast to the soft α-carbon (hardness ~18 GPa). The soft α-carbon provides lubrication, resulting in low friction losses and wear. The nanoscale dispersion of hard Q-carbon and soft α-carbon phases in the Q-carbon nanocomposites enhances the toughness of the coatings. We present detailed

SAMPE Conference Proceedings. Charlotte, NC, May 20-23, 2019. Society for the Advancement of Material and Process Engineering – North America.

structure-property correlations to understand enhancement in the mechanical and magnetic properties of Q-carbon based coatings. The wafer scale-up of DLC films with controlled sp^3 content will be useful for making scalable Q-carbon based longer-lasting protective coatings and electronic devices.

1. INTRODUCTION

1. Introduction

Diamond and diamond-like carbon (DLC) films find applications as coatings and in electronics industry due to their exceptional hardness and thermal conductivity, with high bandgap and low wear rate.[1] DLC films are used as protective coatings against wear and corrosion in optical windows, hard disk drives and micro-electromechanical devices (MEMS). However, DLC films are found to graphitize easily under large loads and moderate temperatures (350^{o}C).[2] These films exhibit short life-span due to poor adhesion, particularly on ferrous substrates comprising 3*d* transition metals due to the weak interposing graphitic layers.[3] The hardness of DLC films can be improved by increasing sp^3 content at the cost of compressive stresses which weaken the film/substrate adhesion. High intrinsic compressive stress limits the coating thickness due to crack formation above critical thickness.[4] Transition elements [5],[6],[7] have been incorporated in DLC films to alleviate the compressive stress, resulting in lower hardness. Even though diamond exhibits tremendous hardness, the CVD grown diamond films on non-diamond substrates are plagued with problems of film chip-off against wear due to graphitization at the substrate/diamond interface.[8] As hard coatings are required to provide 'protection,' while retaining hardness in the mechanical sense with good tribological properties, it is essential to engineer carbon films with high hardness and low compressive stresses.

The susceptibility of carbon films towards sublimation and evaporation losses necessitates minimal exposure of high temperatures. As the heat flow is temporally and spatially confined during nanosecond laser processing, it is an ideal route to melt carbon. The pulsed laser annealing (PLA) process of melting and subsequent quenching is ultrafast (ends in <200 ns) resulting in minimal material loss. By harnessing ultrashort laser pulses, high undercooling can be achieved at the substrate/melt interface, which drives the formation of metastable phases. By utilizing high undercooling in the melt phase, Narayan et al. demonstrated direct conversion of graphitic carbon into pristine diamond by irradiating carbon implanted copper with nanosecond laser pulses.[9] When the undercooling is exceptionally high (>1000 K) the formation of a new state of solid carbon- Q-carbon occurs, with a higher mass density than amorphous carbon. It is a mixture of mostly fourfold sp^3 (75%–85%) bonding with the rest being threefold sp^2 bonded carbon (with distinct entropy)[10]. By controlling the extent of undercooling, the metallic carbon melt can be quenched directly into graphite, diamond or Q-carbon.[11] The Q-carbon has shown many extraordinary properties: *harder* than diamond [10],[12], extraordinary hall effect, room-temperature ferromagnetism[13], field-emission[14], and high-temperature superconductivity[15],[16] upon doping with Boron. Since the first report on the formation of superhard Q-carbon films by laser irradiation, substantial effort has been devoted to scale-up. To scale-up for Q-carbon processing, a low-temperature, large-scale, and versatile process is needed before Q-carbon finds applications in high-temperature superconductivity, field emission, and hard coatings. To achieve industrial order of reliability and consistency in processing, it is necessary to deposit DLC films with consistent sp^3 fraction and controlled thickness over large areas.

In this study, we have deposited DLC films on 2" wafer of *c*-Al_2O_3 by utilizing pulsed laser deposition. PLD is a versatile non-equilibrium-based technique which facilitates the formation of continuous DLC thin films on all electronic materials without the requirement of tuning the deposition conditions for most substrates of interest. The technique described here utilizes room-temperature deposition of DLC films with moderate sp^3 content without delamination. The PLA processed films consist of superhard Q-carbon nanostructures embedded in the soft α-carbon[17] matrix. The amorphous α-carbon is formed when the as-deposited DLC is melted with small undercooling and subsequently quenched. The hardness and mechanical characteristics of the regrown phase has a strong dependence on the extent of undercooling.[17] The contrast between composition and physical behavior of as-grown DLC, Q-carbon, α-carbon, and nanodiamond phases is characterized by Raman spectroscopy, high-resolution scanning electron microscopy and atomic force microscopy (AFM) imaging. With this report, we propose that the non-equilibrium-based methods of PLD and undercooling assisted PLA synthesis methods can be used to fabricate novel Q-carbon based materials for protective coatings and electronic device-based applications.

2. EXPERIMENTATION

2.1 Synthesis of DLC and Q-carbon films

DLC films are deposited on the Al_2O_3 by laser ablation of glassy carbon target, using KrF excimer laser (25 ns pulse duration, 248 nm wavelength, and energy density 3.5-4.0 J cm^{-2}) to a thickness of ~400 nm under the high vacuum of $1x10^{-6}$ Torr inside the pulsed laser deposition (PLD) chamber at room temperature. Subsequently, PLA was performed on DLC films, using a single pulse of ArF Excimer laser with a wavelength of 193 nm and pulse width of 20 ns, at 0.6-

1.0 J cm^{-2} energy density under room temperature and pressure in air. The PLA energy density was controlled using a converging lens, generating a spot size of 1.0 ± 0.01 cm^2.

2.2 Characterization

WITec (Alpha 300M) confocal Raman microscope system with a 532 nm source was utilized to characterize the Raman-active vibrational modes in as-deposited and PLA processed carbon thin films. The Raman spectra were calibrated using single-crystal silicon with a characteristic Raman peak at 520.6 cm^{-1}. High-resolution scanning electron backscattering images were acquired for structural analysis by FEI Verios 460L field-emission scanning electron microscope (FESEM). Evercool Superconducting quantum interference device (SQUID) was employed to analyze magnetic properties for the as-deposited DLC and Q-carbon nanocomposites by probing M *vs* H curves from magnetic fields -1 T to +1 T and 300 K, 100 K and 5 K temperatures. Hysitron Ubi-1 Nanoindenter was utilized to perform *in situ* atomic force microscopy (AFM) and nanoindentation on as-deposited DLC, Q-carbon and α-carbon nanocomposite phases using a Berkovich diamond tip with a radius of curvature of 100 nm, to estimate hardness and Youngs Modulus. Indents were made using an open loop system with symmetric 20 s loading-unloading and 10 s dwell time and 1 mN constant load.

3. RESULTS

3.1 Formation of DLC coating

The DLC films deposited utilizing the highly forward directed plume associated with PLD are prone to delamination due to the inherent stress buildup in the film caused by uneven deposition rates which decrease radially away from plume center. To solve this issue, we utilized a near-point source plume which is spatially broader and leads to lower deposition rates and provides uniform coverage. The plume energetics also control sp^3 content in the as-deposited DLC films.

The Raman spectrum for carbon-based materials comprises of 1340 cm^{-1} (*D* peak), 1560 cm^{-1} (*G* peak), and a small peak at 1140 cm^{-1} associated with strained sp^2 carbon at the interface of sp^3 clusters. Near-point source plume generates ~40-50% sp^3, and forward directed plume can increase sp^3 content to ~90%. Lower sp^3 fraction helps in alleviating stress buildup during wafer scale up for DLC films. The depositions are performed at room temperature to reduce thermal stress and the associated thermal budget for Q-carbon fabrication processing. The sp^3 fraction in the as-deposited DLC films was kept ~40%, which resulted in melting and successful Q-carbon formation upon PLA processing. **Figure 1** shows the optical image of as-deposited 400 nm thick DLC thin film on 2" Al_2O_3 wafer.

3.2 Formation of Q-carbon

The trapped heat flux at the melt-substrate interface triggers superundercooling forming Q-carbon during the regrowth. The ultrafast quenching induces interfacial instability at the melt front, resulting in the nanostructured morphology associated with Q-carbon in **Fig. 2d**. Above the interface, the undercooling is lower which results in the formation of an sp^3 deficient phase-α-carbon. A Voigt peak fitting routine[11, 18] was performed on Q-carbon and α-carbon to determine their sp^3 composition. **Figure 2a and 2b** show the Raman fitting for Q-carbon nanostructures with 82% sp^3 content, whereas α-carbon has a lower sp^3 content 60%. Notably, the *T* peak is absent in α-carbon. As the *T* peak arises from the presence of sp^3 bonded nanoclusters around the sp^2 matrix, its absence in α-carbon signifies that it is a graphitic phase with sp^3 defects present in it. Generally, low undercooling results in the formation of metastable crystalline diamond or thermodynamically stable graphite phases.[11] Under high undercooling, such a rearrangement is truncated, forming physically distinct Q-carbon and α-carbon phases. The transformation of DLC into physically distinct sp^3-rich Q-carbon phase and sp^2-rich α-

carbon matrix highlights nanosecond laser melting and consequent ultrafast quenching during the PLA processing for carbon films. The PLA processing of Q-carbon films leads to modifications in the Raman spectrum as shown in **Fig. 2c**. The sharpening of Raman peak with a shoulder ~1331 cm^{-1} suggests formation of nanodiamonds.

3.3 Microstructural analysis

The large area uniform coverage of Q-carbon filamentary nanostructures upon PLA of DLC films is highlighted in SEM backscattering image shown in **Fig. 2d**. The formation of these filamentary nanostructures in Q-carbon is controlled by the thermal conductivity of the as-deposited DLC films. As thermal conductivity for DLC is directly dependent on sp^3 content, uniform sp^3 composition of DLC films is a necessity to generate the uniform formation of Q-carbon. A sharp interface is noted between the α-carbon and Q-carbon phases in **Fig. 2d**, due to high undercooling and ultrafast quenching of the carbon melt. The PLA of Q-carbon induces remelting and triggers nucleation of nanodiamonds at the Q-carbon nanostructures. The nanodiamonds preferentially nucleate at the triple points, where the filamentary structures of Q-carbon intersect. The high-resolution SEM image in **Fig. 2e** highlights the nucleation of nanodiamonds from a Q-carbon filamentary nanostructure. The multiple-shot PLA processing leads to the formation of microdiamonds as Q-carbon gives way to complete diamond growth.[19] As the PLA process ends in less than 200 ns, such extremely high growth rates can only be achieved in the liquid phase where diffusivity reach as high as 10^{-4} cm^2/s.

In solids, thermal conductivity (K_T) has contributions from electrons (K_e) and phonons (K_P), i.e., $K_T = K_P + K_e$. Graphitic carbon films have $K_P \sim 0.3$ $Wm^{-1}K^{-1}$ and high sp^3 disordered DLC thin films have $K_P \sim 10$ $Wm^{-1}K^{-1}$. which forms a homogenous melt ~4000 K. [20] The carbon melt is metallic in nature, and its properties can be approximated by the free electron gas model. [21, 22]

Post-PLA, and the structure of regrown solid is dependent on the solid regrowth velocity from the undercooled melt state. The quenching rate is thermodynamically driven by the thin film and substrate thermal conductivity. [23] On decreasing the substrate thermal conductivity, it traps heat flux leading to an increase in temperature at the interface. Further, an increase in the sp^3 content of the DLC thin film results in enhancement of bulk thermal conductivity at the regrown solid-liquid interface, increasing thermal losses at the surface. Formation of amorphous Q-carbon occurs due to the rise in interfacial instability above the critical undercooling (ΔT_u^c); $\Delta T_u^c > T_m^{dia} - T_m^{\alpha}$, where T_m^{dia} and T_m^{α} are the melting points for diamond and amorphous carbon, respectively.[24] Due to the difference between the Gibbs free energy for disordered amorphous carbon and crystalline diamond, it is thermodynamically possible to attain amorphous regrowth at the melt interface, above ΔT_u^c. [23, 25]

3.4 Ferromagnetism in Q-carbon

The ultrafast regrowth of from the superundercooled melt phase during PLA processing generates an unprecedented number of $p\pi$ dangling bonds in Q-carbon. These bonds contain unpaired spins generating ferromagnetism inside the Q-carbon matrix. Ferromagnetism arises in carbon derivatives due to the positive value of exchange energy and magnetic coupling between unpaired electrons in π-orbitals. On PLA processing DLC films with ~52% sp^3 content, the formation of Q-carbon occurs. [10, 13] The saturation magnetization for Q-carbon at 5 K was determined to be 20.00 emu g^{-1}[13] which increases to 22.40 emu g^{-1} in Q-carbon nanocomposites (**Fig. 3**) which forms on annealing DLC with 75% sp^3 content. In Q-carbon, there is a high density of electronic states near the Fermi level, indicating a significant number of dangling bonds. Due to the small cellular size of Q-carbon in nanocomposites, the average magnetic domain size decreases, thereby generating more phase boundaries. The phase boundaries act as

pinning centers, increasing the activation energy required for flipping the moment upon introduction of the magnetic field. The increase in activation energy is apparent from the rise in coercivity from 80 Oe in Q-carbon[10] to 140 Oe in Q-carbon nanocomposites at 300 K. Notably, DLC also has disordered sp^2-sp^2 bonds truncated with sp^2-sp^3 bonding. Such disorder should generate unpaired electrons, inducing ferromagnetic ordering. However, we observe diamagnetism in DLC as shown in the inset of **Fig. 3**, highlighting the fact that it is a physical mixture of sp^2 and sp^3 bonds.

3.5 Mechanical properties of Q-carbon

Figure 4a depicts the AFM scan of DLC thin films. Due to shrinkage in volume on quenching from the superundercooled melt state, the Q-carbon nanostructures are shallow in depth as shown in **Fig. 4b.** The step shrinkage at Q-carbon nanostructures is ~40 nm consistently around the specimen. The ensemble thickness of Q-carbon nanocomposites is ~80 nm. The Q-carbon nanostructures are embedded in the thin α-carbon matrix. In the Raman spectra, SEM, and AFM imaging, stark differences are evident between the physical properties of α-carbon and Q-carbon phases. Interestingly, on probing the individual Q-carbon filamentary nanostructures using a sub-angstrom modulated nanoindentation technique, it revealed that Q-carbon is >40% higher hardness than diamond.[12] The hardness of as-deposited DLC is estimated to be 24 GPa with Young's modulus of 325 GPa. It shows a higher depth of penetration (35 nm) on applying 1 mN load as shown in **Figure 5d**. The hardness of ensemble Q-carbon nanocomposites to be 67 GPa, with a Young's modulus of 840 GPa. The hardness of Q-carbon nanostructures can be qualitatively ascertained by the small depth of penetration in the loading-unloading curve in **Fig. 4c.** The hardness of α-carbon phase is determined to be 18 GPa with a Young's Modulus 280 GPa. The depth of penetration for α-carbon is determined to be 54 nm as shown in **Fig. 4e**. The

Q-carbon nanocomposites have an sp^3 deficient α-carbon phase, which acts as the lubricant reducing of friction coefficient to ~0.09.[17] In comparison, DLC has a friction coefficient of 0.12–0.2, depending on the sp^3 content, which further worsens to 0.4 after continuous wear cycles for tests performed in ambient air conditions (relative humidity RH = 50-70%) at room temperature with load 2-5 N. [26, 27] An essential requirement for reducing the wear rate is the presence of an adhesive interfacial layer between the substrate andcrystalline/amorphous coating, which serves the dual purpose of enhancing adhesion and stress-relief. The superhard Q-carbon nanostructures anchor the lubricating α-carbon matrix with the underlayer performing the stress-relief.[28] As this interfacial layer of Q-carbon forms by ultrafast quenching of the super undercooled carbon melt, it has excellent adhesion with the sapphire substrate.

4. CONCLUSIONS

By employing plume energetics during pulsed laser deposition, we created large-area Q-carbon by nanosecond laser melting of wafer-scale DLC films with the uniform sp^3 composition at ambient temperature. On laser irradiation, uniform formation of large-area Q-carbon is observed due to ultrafast quenching of the super undercooled carbon melt. Further laser irradiation led to the conversion of Q-carbon into nanodiamonds at the tip of filamentary nanostructures. The morphology of Q-carbon and nanodiamonds are correlated with the structure using Raman spectroscopy, SEM and AFM imaging. Also, the Q-carbon nanocomposite coatings show intrinsic ferromagnetism with 20 emu g^{-1} saturation magnetization and 140 Oe coercivity at 300 K. These studies show that Q-carbon nanocomposites have superior hardness, lower wear rate and higher packing fraction as compared to DLC coatings. We envisage that the wafer scale-up of DLC and Q-carbon films will result in furthering the research on carbon-based materials for coating applications.

Acknowledgments

We are grateful to Fan Family Foundation Distinguished Chair Endowment for Prof. J. Narayan. This research work was performed under the National Science Foundation (Award Number DMR- 1560838, DMR- 1735695).

5. REFERENCES

[1] Robertson J. Diamond-like amorphous carbon. Materials Science and Engineering: R: Reports 2002;37:129-281.

[2] Wang D-Y, Chang C-L, Ho W-Y. Oxidation behavior of diamond-like carbon films. Surf Coat Technol 1999;120:138-44.

[3] Chen X, Narayan J. Effect of the chemical nature of transition-metal substrates on chemical-vapor deposition of diamond. J Appl Phys 1993;74:4168-73.

[4] Gille G, Rau B. Buckling instability and adhesion of carbon layers. Thin Solid Films 1984;120:109-21.

[5] Jarratt M, Stallard J, Renevier N, Teer D. An improved diamond-like carbon coating with exceptional wear properties. Diamond Relat Mater 2003;12:1003-7.

[6] Fryda M, Taube K, Klages CP. Nanometer indentation measurements on metal-containing amorphous hydrogenated carbon films (Me□C: H). Vacuum 1990;41:1291-3.

[7] Bewilogua K, Cooper CV, Specht C, Schröder J, Wittorf R, Grischke M. Erratum to: “Effect of target material on deposition and properties of metal-containing DLC (Me-DLC) coatings”: [Surf. Coat. Technol. 127 (2000) 224–232]1The publisher regrets that during the processing of this article errors were introduced. The correct version, reprinted in full appears in these pages.2PII of original article: S0257-8972(00)00666-6.1,2. Surf Coat Technol 2000;132:275-83.

[8] Sachan R, Bhaumik A, Pant P, Prater J, Narayan J. Diamond film growth by HFCVD on Q-carbon seeded substrate. Carbon 2019;141:182-9.

[9] Narayan J, Godbole V, White C. Laser method for synthesis and processing of continuous diamond films on nondiamond substrates. Science 1991;252:416-8.

[10] Narayan J, Bhaumik A. Novel phase of carbon, ferromagnetism, and conversion into diamond. J Appl Phys 2015;118:215303.

[11] Gupta S, Sachan R, Bhaumik A, Pant P, Narayan J. Undercooling driven growth of Q-carbon, diamond, and graphite. MRS Communications 2018; 8: 533-540.

[12] Narayan J, Gupta S, Bhaumik A, Sachan R, Cellini F, Reido E. Q-carbon is harder than diamond MRS Communications 2018; 8: 428-436.

[13] Bhaumik A, Nori S, Sachan R, Gupta S, Kumar D, Majumdar AK, et al. Room-Temperature Ferromagnetism and Extraordinary Hall Effect in Nanostructured Q-Carbon: Implications for Potential Spintronic Devices. ACS Applied Nano Materials 2018.

[14] Narayan J, Bhaumik A, Gupta S, Haque A, Sachan R. Progress in Q-carbon and related materials with extraordinary properties. Materials Research Letters 2018;6:353-64.

[15] Bhaumik A, Sachan R, Narayan J. High-Temperature Superconductivity in Boron-Doped Q-Carbon. ACS nano 2017.

[16] Bhaumik A, Sachan R, Gupta S, Narayan J. Discovery of High-Temperature Superconductivity (T c= 55 K) in B-Doped Q-Carbon. ACS nano 2017;11:11915-22.

[17] Gupta S, Sachan R, Bhaumik A, Narayan J. Enhanced mechanical properties of Q-carbon nanocomposites by nanosecond pulsed laser annealing. Nanotechnology 2018;29:45LT02.

[18] Gupta S, Moatti A, Bhaumik A, Sachan R, Narayan J. Room-temperature ferromagnetism in epitaxial titanium nitride thin films. Acta Mater 2019;166:221-30.

[19] Narayan J, Bhaumik A. Novel synthesis and properties of pure and NV-doped nanodiamonds and other nanostructures. Materials Research Letters 2016;5:242-50.

[20] Shamsa M, Liu W, Balandin A, Casiraghi C, Milne W, Ferrari A. Thermal conductivity of diamond-like carbon films. Appl Phys Lett 2006;89:161921.

[21] Heremans J, Olk C, Eesley G, Steinbeck J, Dresselhaus G. Observation of metallic conductivity in liquid carbon. Phys Rev Lett 1988;60:452.

[22] Steinbeck J, Dresselhaus G, Dresselhaus M. The properties of liquid carbon. Int J Thermophys 1990;11:789-96.

[23] Cullis A, Webber H, Chew N, Poate J, Baeri P. Transitions to defective crystal and the amorphous state induced in elemental Si by laser quenching. Phys Rev Lett 1982;49:219.

[24] Gupta S, Bhaumik A, Sachan R, Narayan J. Structural Evolution of Q-Carbon and Nanodiamonds. JOM 2018;70:450-5.

[25] Spaepen F, Turnbull D, Ferris S, Leamy H, Poate J. Laser-Solid Interactions and Laser Processing. AIP Conf Proc1979.

[26] Grill A. Tribology of diamondlike carbon and related materials: an updated review. Surf Coat Technol 1997;94:507-13.

[27] Grill A. Diamond-like carbon: state of the art. Diamond Relat Mater 1999;8:428-34.

[28] Voevodin A, Walck S, Zabinski J. Architecture of multilayer nanocomposite coatings with super-hard diamond-like carbon layers for wear protection at high contact loads. Wear 1997;203:516-27.

Figures

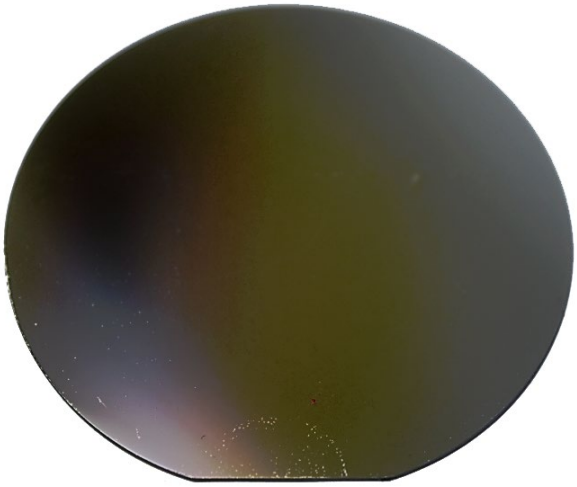

Figure 1. (a) Optical image of diamond-like carbon coating deposited on 2-inch Al_2O_3 wafer by pulsed-laser deposition.

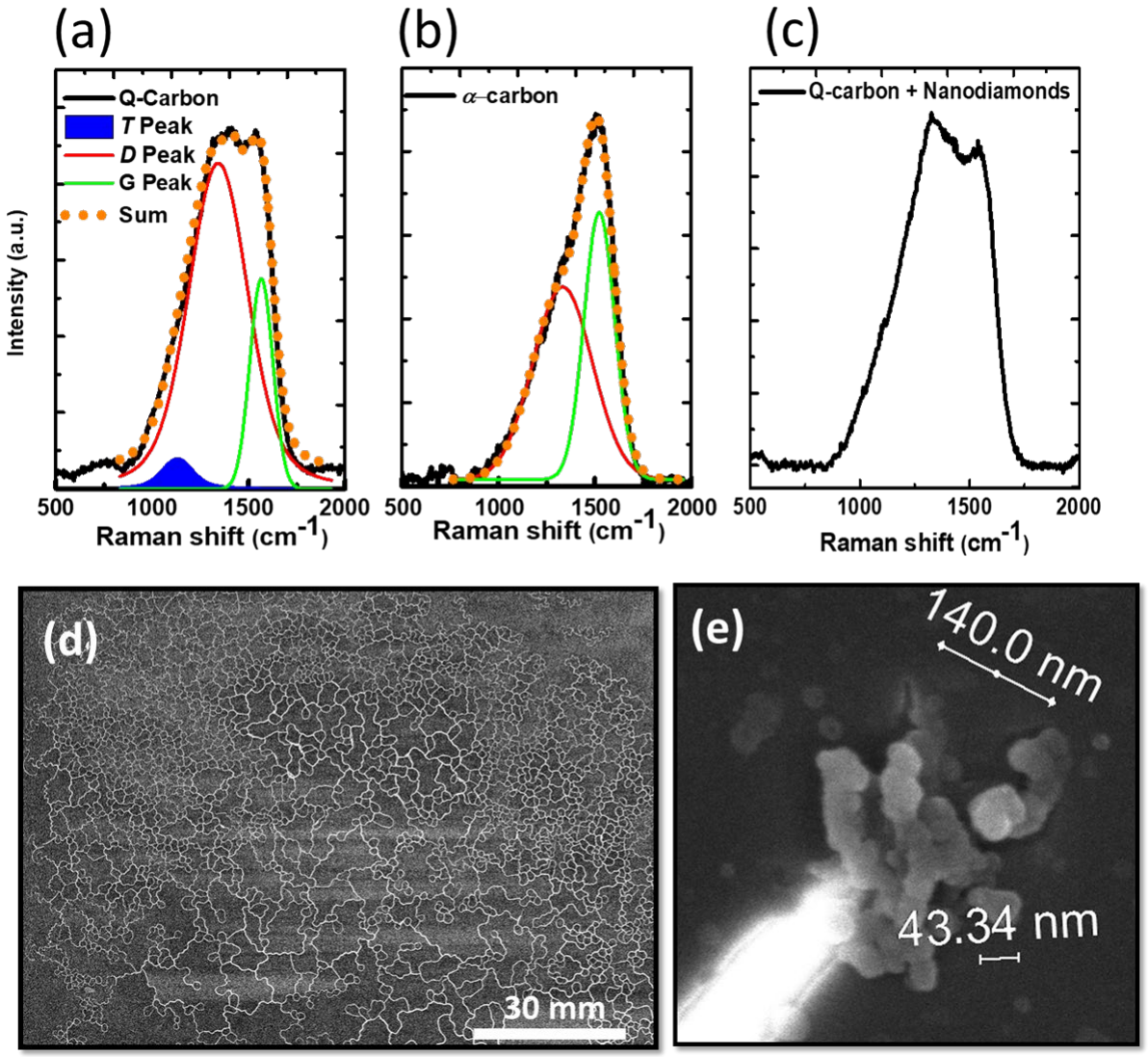

Figure 2. Raman spectra highlighting the formation of distinct (a) Q-carbon and (b) α-carbon phases, (c) shows the Raman spectrum acquired from re-irradiated Q-carbon, prominently containing Q-carbon and nanodiamonds. (c) FESEM imaging for laser irradiated large-area Q-carbon nanostructures formed after PLA processing of moderate sp^3 (48%) DLC. (d) reveals converison of Q-carbon into nanodiamonds at the tip of Q-carbon filamentary nanostructure.

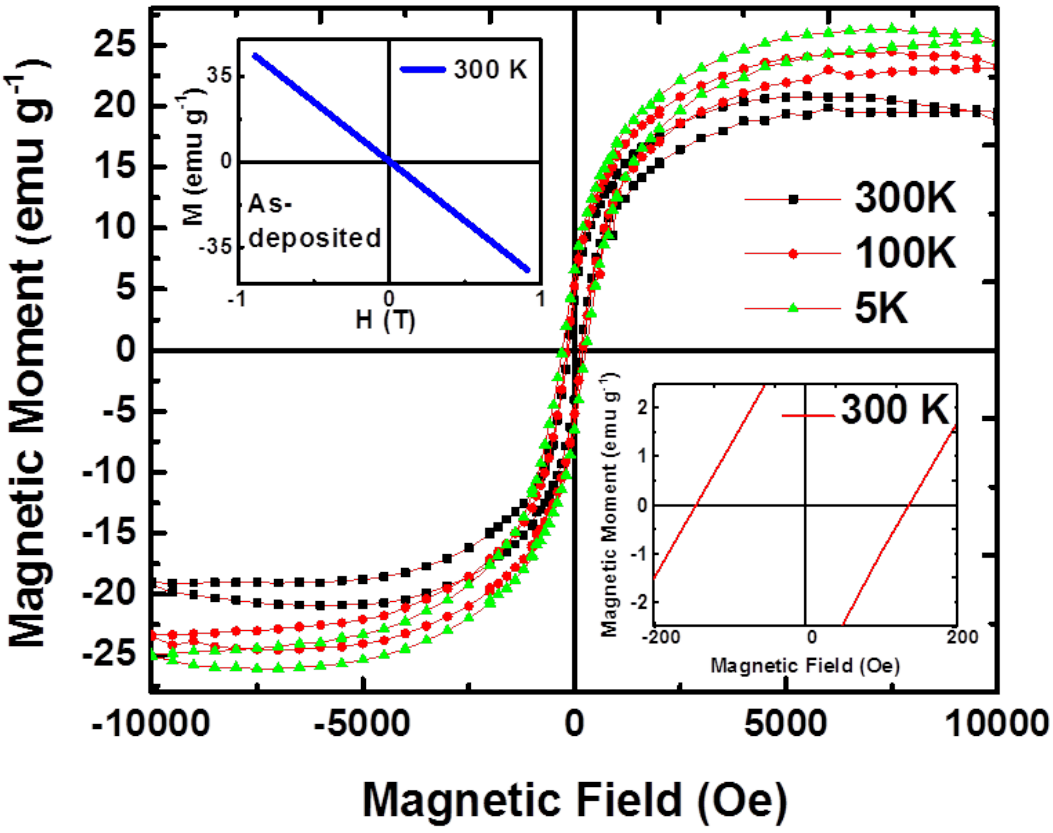

Figure 3. Isothermal M-H plots for Q-carbon nanocomposites at various temperatures (300 K, 100 K and 5 K)) with inset (bottom-right) illustrating the finite coercivity of 140 Oe at 300 K. The inset in top-left reveals the diamagnetic nature of as-deposited DLC at 300 K.

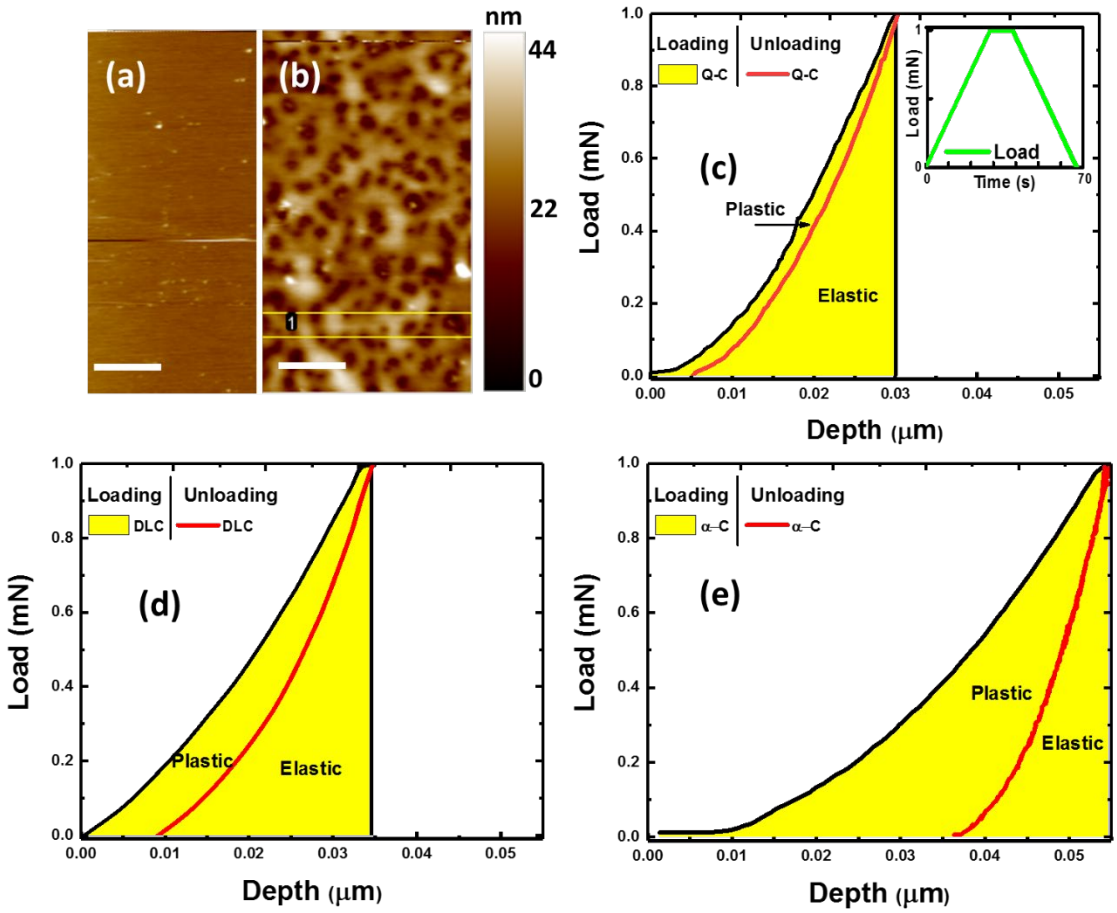

Figure 4. AFM scans showing the morphology of (a) as-deposited DLC; (b) Q-carbon nanocomposites; The scale bar in (a) and (b) is 2 μm. (c) Loading and unloading curves for Q-carbon nanocomposites (Q-C) with a hardness of 67 GPa; (d) high sp^3 DLC exhibiting a hardness of 24 GPa; and (e) α-carbon with a hardness of 18 GPa.